Structure of the Dimyristoylphosphatidylcholine Vesicle and the Complex Formed by Its Interaction with Apolipoprotein C-III: X-ray Small-Angle Scattering Studies†

Peter Laggner,* Antonio M. Gotto, Jr., and Joel D. Morrisett‡

ABSTRACT: Single bilayer vesicles of dimyristoylphosphatidylcholine have been investigated by small-angle X-ray scattering at 28 °C. The results indicate that these vesicles are hollow spherical shell structures with an outer radius of approximately 12 nm and a molecular weight of (3.2 ± 0.5) × 10^6. The shell was found to be 4.4 ± 0.2 nm thick with a cross-sectional electron-density profile characteristic for a single phospholipid bilayer. Upon interaction of these vesicles with apolipoprotein C-III from human very low density lipoproteins at a protein/lipid ratio greater than 0.08 (g/g), a complex containing 0.25 g of protein/g of lipid, with molecular weight of (3.9 ± 0.4) × 10^5, is formed. The shape analysis indicates a highly asymmetric particle with an internal partition of low and high electron density resembling that produced by a bilayer structure. Model calculations and curve-fitting procedures show good agreement between the experimental scattering curve and that computed for an oblate ellipsoidal structure with dimensions of 17 × 17 × 5 nm and a 1 nm thick shell of high electron density surrounding the core of low electron density.

The physicochemical characterization of lipid–protein complexes obtained by recombination of isolated apolipoproteins with defined lipid systems has proven to be an instructive method for gaining a clearer understanding of the nature of lipid–protein interactions in native lipoprotein and membrane systems. Among the best characterized recombinant systems in the field of plasma lipoproteins are the complexes formed between apolipoprotein C-III (apoC-III[1]) from human very low density lipoproteins and phoshatidylcholines. Spectroscopic studies have provided a wealth of information about the mutual physical effects of lipid–protein interaction at the molecular level (Pownall et al., 1974, 1977; Träuble et al., 1974; Morrisett et al., 1974; Novosad et al., 1976; Aune et al., 1977). It has been shown that the structure of the resulting lipid–protein complexes depends on several factors such as the fatty acyl chain composition of the phosphatidylcholines (Pownall et al., 1977), the lipid–protein mass ratio (Morrisett et al., 1974; Aune et al., 1977), and the state of dispersion of the phospholipids before recombination (Morrisett et al., 1977). In the case of apoC-III and dimyristoylphosphatidylcholine (DMPC) vesicles, it was found that, above a protein–lipid mass ratio of 0.08 (g/g), their interaction leads to the formation of particles which are considerably smaller than the original DMPC vesicles. Average values of 8.0 nm for the hydrodynamic radius and 442 000 for the molecular weight were obtained by a combination of ultracentrifugal, light scattering, and gel filtration methods and led to the presentation of several possible models for this complex. The experimental evidence did not, however, allow an unambiguous structural description.

The analysis of X-ray small-angle scattering data to be described in the present article provides further quantitative information about the size, shape, and internal structure of DMPC vesicles and the DMPC–apoC-III complex. The results confirm and amplify many of the previous findings from hydrodynamic studies by Aune et al. (1977) and represent independent evidence for the description of the molecular structure of phospholipid bilayer vesicles and apolipoprotein–phospholipid complexes.

Experimental Section

Materials

ApoC-III containing one residue of sialic acid was isolated from very low density lipoproteins as indicated previously (Morrisett et al., 1974). DMPC was obtained from Sigma Chemical Co. Single bilayer vesicles of this phospholipid and complexes formed by its interaction with apoC-III were prepared as described earlier (Aune et al., 1977). After chromatography on Sepharose 6B, these species were concentrated by ultrafiltration in an Amicon 8 M microcell equipped with an XM100 membrane. Samples were centrifuged at 20000*g* for 30 min to remove any particulate material which formed during concentration.

Methods

X-ray Instrumentation. A slit collimation camera (Kratky, 1958) was adjusted on the line-focus (0.01 × 1.0 cm) window of a modified Rigaku Denki RU 500 VS rotating Cu anode generator (Janosi and Degovics, 1976) operated at 50 kV and 400 mA. Entrance slit widths of 60 and 100 μm were used alternatively, depending on the angular range of interest. The scattering intensities were registered at a distance of 21.5 cm from the sample by a proportional counter using a programmable electronic step scanner (Leopold, 1968). The integral length of the primary beam in the plane of registration was 4.0 cm. Thin-walled Mark capillaries (Hilgenberg, Germany) were used to hold the samples. All measurements were performed at 28 °C, controlled to ±0.1 °C by a Peltier cuvette (Leopold, 1969). Generally 10^5 pulses were counted at each point of the scattering curves, both for the sample and for the blank exposures. The statistical evaluation of the data

† From the Institut für Röntgenfeinstrukturforschung der Österreichischen Akademie der Wissenschaften und des Forschungszentrums, Graz, Austria (P. L.), and the Departments of Medicine and Biochemistry (A.M.G., J.D.M.), Baylor College of Medicine, The Methodist Hospital, Houston, Texas 77030. *Received May 22, 1978.* This work was supported by the Österreichischer Fonds zur Förderung der Wissenschaftlichen Forschung and by grants from the National Heart, Lung, and Blood Institute for a National Heart and Blood Vessel Research and Demonstration Center (HL-17269-03) and for a General Clinical Research Center (RR-00350). This work has also benefited from a grant by the American Heart Association, Texas Affiliate, to J.D.M.

‡ Established Investigator of the American Heart Association (1974–1979).

[1] Abbreviations used: DMPC, dimyristoylphosphatidylcholine; apoC-III, an apolipoprotein of very low density lipoproteins from human plasma (M_r 9300) containing one residue each of galactose, galactosamine, and sialic acid.

0006-2960/79/0418-0164$01.00/0

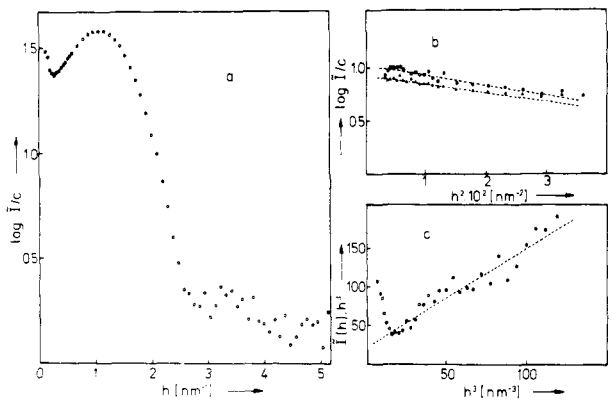

FIGURE 1: (a) Scattering intensities $\tilde{I}/c$ of a solution of DMPC single bilayer vesicles (36 mg/mL) uncorrected for the collimation geometry (T = 28 °C). (b) Guinier plot of the uncorrected scattering intensities $\tilde{I}/c$ of DMPC vesicles at the lowest scattering angles. Concentrations: (○) 12 mg/mL; (▲) 36 mg/mL. (c) Asymptotic trend proportional to h^{-3} of the uncorrected scattering intensities $\tilde{I}/c$ (36 mg/mL) towards large angles.

(Zipper, 1969) and the corrections for the primary beam geometry (desmearing; Kratky et al., 1960) as well as for the influence of the Cu Kβ radiation were performed by the method of Glatter (1977) with the Univac 494 computer of the Rechenzentrum Graz.

Partial Specific Volume Measurements. The apparent partial specific volumes at chemical equilibrium were determined at 28.0 °C by precision densimetry (Kratky et al., 1973) using a modified Mettler–Paar densimeter, DMA 601, operating with two oscillators in the reference mode (Laggner and Stabinger, 1976). This technique greatly reduces errors arising from residual temperature fluctuations of the temperature control unit and allows determination of densities to an accuracy of $\pm 10^{-6}$ g/cm^3. Thus, the error in the calculated $\bar{v}$ values is controlled principally by the accuracy in determination of solute concentration. Assuming relative errors in solute concentration of ±3%, this would in the given cases lead to errors in the apparent partial specific volumes of $\pm 2.10^{-3}$ g/cm^3. The sample concentrations as measured by protein absorbance at 280 nm (E_{280} = 2.16 mL mg^{-1} cm^{-1}; Aune et al., 1977) and by phospholipid determination according to the method of Bartlett (1959) were in the range of 10–30 mg/mL. In this range the concentration dependence of $\bar{v}$ was found to be negligible.

Electron Microscopy. Samples of DMPC vesicles and of the DMPC–apoC-III complex at concentrations of 0.1–1.0 mg/mL were mixed with equal volumes of 2% sodium phosphotungstate at pH 6.8 and applied to hydrophilized (Jakopitsch & Horn, 1962) carbon-coated copper grids. Electron micrographs were obtained with a Philips EM 300 at the Zentrum für Elektronenmikroskopie, Graz (courtesy of Drs. Ingolic and Geymayer).

Results and Discussion

Structure of DMPC Vesicles. The scattering curve of a 36 mg/mL solution of DMPC vesicles at 28 °C is shown in Figure 1a. Measurements were begun within 2 h after column fractionation and concentration of the selected fractions. The time required to accumulate the data in six consecutive scans with a total of 1.2×10^5 counts at each point was 20 h, and within this time no systematic drifts were observed. The mean relative error after subtraction of the blank scattering was less than 2% in the angular range of $h < 2$ nm^{-1} ($h = 4\pi \sin\theta/\lambda$; 2θ, scattering angle; λ = 0.154 nm) and in the low intensity outer part less than 10%. In a second, simultaneous experiment, the innermost part of the scattering curve was measured with an identical sample at concentrations of 36 and 12 mg/mL. As shown in the plot of log $\tilde{I}/c$ vs. h^2 ($\tilde{I}$, uncorrected intensities) (Figure 1b), this part of the scattering curves can be approximated by single Gaussian functions, indicating that the system is, within the limits of detection, monodisperse (Guinier and Fournet, 1955). However, this statement can only be made for the angular range covered by this experiment ($h > 0.06$ nm^{-1}) since small amounts of large aggregates as observed in the light scattering studies of Aune et al. (1977) would be detectable only at even smaller angles. The apparent radii of gyration, $\tilde{R}$, calculated from the slopes of the straight lines according to

$$\tilde{R}^2 = (3/\log e)(-\tan \alpha) \qquad (1)$$

are 7.4 and 7.9 nm for c = 36 and 12 mg/mL, respectively. During the total 4 h of exposure, in five consecutive scans the scattering intensities at angles of $h < 0.09$ nm^{-1} increased systematically, suggesting that aggregation occurred at a low rate. The intensities in Figure 1b are the average values over all five scans. The relative mean errors increased from 5% at h = 0.09 nm^{-1} to 17% at h = 0.06 nm^{-1}. Therefore, we did not attempt to eliminate the concentration-dependent interparticle interference effects by extrapolation, but used the data obtained at the lower concentration (12 mg/mL) for subsequent evaluation of the experimental results. It can be assumed that the errors created by this approach are negligible within the limits of resolution obtained by the structural analysis described in the following. Figure 1c shows that the scattering curve in its outer part follows a course which can be separated into the theoretically expected term proportional to h^{-3} (Porod, 1952) and a constant term (Luzzati et al., 1961; Kratky, 1963). The constant term arising from the short-range electron density fluctuations and possibly also from errors in the blank subtraction was subtracted from the experimental curve.

The basis for the structural interpretation of the results is given by the real-space distance distribution function $p(r)$ which is related to the desmeared scattering curve $I(h)$ via Fourier transformation, according to

$$p(r) = \frac{1}{2\pi^2} \int_0^\infty I(h) hr \sin(hr)\, dh \qquad (2)$$

The function $p(r)$ corresponds to the frequency of occurence of any given distance r within one particle between two different volume elements dv weighted by the relative electron densities. It is related to the "characteristic" correlation function $\gamma(r)$ of the particle (Porod, 1948) by $p(r) = \gamma(r)r^2$ (Guinier and Fournet, 1955). A numerical method described in detail elsewhere (Glatter, 1977) gives in one operation both the desmeared scattering curve $I(h)$ and $p(r)$ directly from the experimental intensities $\tilde{I}(h)$. In this procedure, the assumption is made that $p(r) = 0$ beyond an arbitrarily chosen distance D_{max}. If, in a given system, the maximum particle dimension D can be estimated from other physical information, such as the Stokes' radius or from electron microscopy, the value of D_{max} is favorably chosen as approximately 1.2D. Within the range of $0 < r < D_{max}$ the distance distribution function is then defined by the linear combination of a finite number N of cubic B-Spline functions (Greville, 1969). The optimal value for N is chosen such that, on the one hand, the fit between the analytically smeared solution function $\tilde{I}(h)_{approx}$ and the experimental result $\tilde{I}(h)$ is sufficiently good but that, on the other hand, the resulting $p(r)$ function does not suggest an unreasonably high resolution. In the present case, 30 Spline functions were used, and the value of D_{max} was chosen as 30 nm on the basis of the reported hydrodynamic diameter of 25

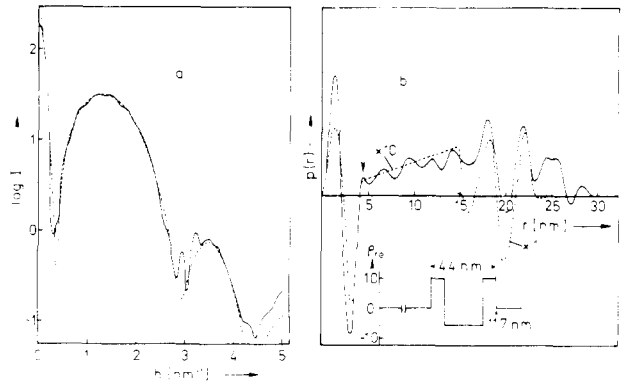

FIGURE 2: (a) Desmeared scattering curve of DMPC vesicles obtained from the experimental data underlying a maximum intraparticle distance D_{max} of 30 nm (solid line). Broken line corresponds to the desmeared scattering curve obtained by assuming a leaflet structure with no tangential contributions and a maximum distance of 6 nm for the cross-sectional transform $\gamma_t(r)$ (see Figure 6). (b) Full line: distance distribution function $p(r)$ defined by 30 cubic Spline functions in the range of $0 < r < 30$ nm related to $I(h)$ [solid line in (a)] by eq 2. Broken line: theoretical distance distribution function $p(r)$ of a spherical shell structure with the dimensions and electron density (ρ_{rel}) profile shown in the insert.

nm (Aune et al., 1977). The resulting desmeared scattering curve and the corresponding distance distribution function $p(r)$ are shown in Figure 2.

The distance distribution function $p(r)$ (Figure 2b) is characteristic of hollow spherical particles with strong positive-to-negative fluctuations within the shell. The thickness of the shell can be estimated from the value of r at which the $p(r)$ function passes from the large initial positive–negative oscillation into the adjacent ascending region of smaller oscillations (Laggner et al., 1977). For DMPC vesicles at 28 °C, this point lies at approximately 4.4 nm as indicated by the arrow in Figure 2b. In theory, the overall particle diameter should be determinable from the point at which $p(r)$ finally remains zero. In practice, several experimental conditions prevail which prevent a precise determination of the largest intraparticle distance: The principal reasons are the limited accuracy with which the scattering intensities at the very lowest angles [which primarily determine $p(r)$ at the largest distances] can be measured and concentration effects which cannot be eliminated; the presence of minor amounts of aggregates as well as size and shape heterogeneities certainly also have a detrimental influence on the data at high values of r; finally, residual termination effects and artifacts arising from the limited number of approximation functions (which also contribute to the oscillations in the range of r between 5 and 16 nm) may also obscure the maximum particle size. Thus, from the data in Figure 2b, we estimate the maximum diameter of the DMPC vesicles to be 24 to 26 nm, which is in good agreement with our previously determined hydrodynamic diameter of 25 nm (Aune et al., 1977). These experimental data are similar to the theoretical $p(r)$ function of a hollow spherical particle with 23.4-nm outer diameter, 4.4-nm shell thickness, and an electron density profile across the shell approximating that expected for a lipid bilayer. Figure 2b clearly shows two peaks at 18 and 22 nm separated by a pronounced negative trough which is good evidence for the spherical shell structure. However, there are significant differences in the relative heights of these signals. From these and other differences we must infer some degree of variation in vesicle size which is known to correlate with the elution volume of the phospholipid vesicles from the gel filtration column (Andrews et al., 1975). We estimate that the half-width of this distribution is <2 nm. A precise evaluation of this distribution, however, would require more experimental data and would have to be based on the assumption of ideal rigidity and uniform shapes of the vesicles.[2]

From the absolute scattering intensity at zero angle $I(0)$ it is possible to calculate a "molecular weight" of the vesicles (Kratky et al., 1951; Kratky, 1963). According to the relation

$$M = \frac{I(0)}{P_0} \frac{21.0a^2}{(\Delta z)^2 dc} \tag{3}$$

in which $I(0)/P_0$ is the scattering intensity at zero angle relative to the primary intensity P_0 [$I(0)/P_0 = 4.5 \times 10^{-5}$, as determined by the method of Pilz and Kratky (1967)], a is the sample-to-detector distance (21.5 cm), Δz is the number of excess gram-electron per gram of solute (1.23×10^{-2}), and c and d are the sample concentration and thickness, respectively. Because of the low electron density difference between solute and solvent, a precise determination of $(\Delta z)^2$ is very difficult. This value is calculated from the chemical composition and the apparent partial specific volume found by precision densimetry (Kratky et al., 1973). At 28 °C, $\bar{v}$ of DMPC vesicles was found to be 0.969 ± 0.002 cm^3/g as the mean value for five individual vesicle preparations. Based on this number, we obtain a value for M of $(3.2 \pm 0.5) \times 10^6$. Previous sedimentation analysis on similar preparations has resulted in a molecular weight value of 2.73×10^6 (Aune et al., 1977). Using the $\bar{v}$ of 0.972 cm^3/g reported previously (Aune et al., 1977) and assuming an identical solvent density of 1.0009 g/cm, a value of $M = 4.3 \times 10^6$ is calculated. Thus, the errors involved in the determination of $\bar{v}$ impose a critical limitation on the precision of the calculation of molecular weight; therefore the present data allow only a crude estimation.

Information about the cross-sectional structure can be obtained from an analysis of the "thickness factor" $I_t(h)$, according to the relation

$$I_t(h) = I(h)h^2 \tag{4}$$

where I_t represents the scattering arising from the cross-sectional structure (Porod, 1948). This relation holds for lamellar structures in which the thickness is small compared to the overall particle dimensions. However, it has been shown on the fatty acid synthetase complex (Pilz et al., 1970) that this treatment can also be applied to spherical shell structures in which the shell thickness is of the order of 20 to 30% of the outer radius. Wilkins et al. (1971) were the first to introduce this approach into the analysis of X-ray scattering results from phospholipid vesicles, and in a recent report, its usefulness was demonstrated in elucidating the structure of the pathological lipoprotein, LP-X, which also displays vesicular structure (Laggner et al., 1977). In the present work we obtained the thickness factor, $Ih^2(h)$ (Figure 3a), directly from the original data of $\tilde{I}(h)$ by an analogous procedure as described above for the process of desmearing and calculation of $p(r)$. In this case, a set of 12 cubic spline functions were used to define the

[2] The heterogeneity in vesicle size is also responsible for the fact that the expected intensity fluctuations with a period of $\Delta h = \pi/R$ for spherical shell structures with a radius R are largely smeared out. However, an estimation based upon the periodicity of $\Delta h = 0.3$ nm^{-1} apparent from Figure 2a indicates a radius of 10.5 nm which, considering the errors involved in this estimation, is in good agreement with the results inferred from the $p(r)$ function. It is noteworthy, however, that the overall dimensions derived from the $p(r)$ function do not depend on this periodicity but are largely determined by the slope of the primary maximum (Laggner, 1977).

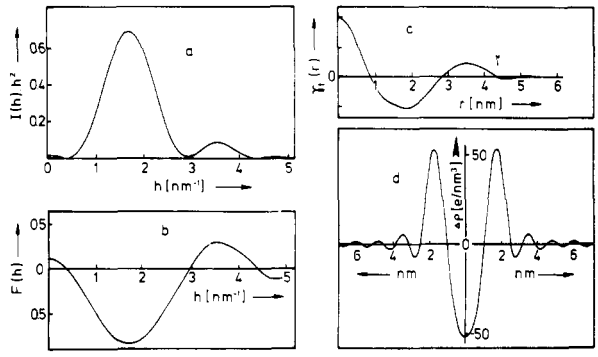

FIGURE 3: (a) Thickness factor $I(h)h^2$ of DMPC vesicles obtained from the uncorrected data by assuming a one-dimensional cross-section distance distribution function $\gamma_t(r)$ limited to the dimensions $0 < r < D_{max}$, where $D_{max} = 6$ nm. (b) Thickness amplitudes $F(h) = \pm I(h)^{0.5}h$ obtained from $I(h)h^2$ in (a). (c) Distance distribution function $\gamma_t(r)$ related to $I(h)h^2$ by eq 5. (d) Electron density profile $\Delta\rho(r)$ across the bilayer thickness obtained from $F(h)$ according to eq 7.

real-space correlation function $\gamma_t(r)$ of the lamellar thickness in the range of $0 < r < 6$ nm. The function $\gamma_t(r)$ is related to the thickness factor by the cosine transformation

$$\gamma_t(r) = \frac{1}{\pi}\int_0^\infty I(h)h^2 \cos(hr)\, dh \qquad (5)$$

The corresponding scattering function $I(h)$ and the cross-sectional correlation function $\gamma_t(r)$ are shown in Figures 2a and 3c, respectively. In analogy to the three-dimensional distance distribution function $p(r)$, the thickness of the shell can be inferred from the point at which $\gamma_t(r)$ vanishes. Thus, a value of 4.4 nm is obtained from Figure 3c (see arrow). It should be emphasized that the information upon which the function $\gamma_t(r)$ is based, the function $Ih^2(h)$, is practically unaffected by the experimental errors at the lowest angles and is determined mainly by the relative heights and positions of the broad secondary maxima (see Figure 3a). An advantage of the direct determination of the cross-section factor from the experimental function $\tilde{I}(h)$ lies in the possibility of estimating the propagation of the statistical error on $\gamma_t(r)$. In the present case the $\gamma_t(r)$ function is affected by an almost constant error band of 2% of the maximum value at $r = 0$. Beyond the crossover at 4.4 nm the oscillations arising from unavoidable termination effects are about of the same magnitude as the statistical error and hence the thickness of the lamella can be given as 4.4 ± 0.2 nm (see footnote 3).

By integration of $\gamma_t(r)$ according to

$$I(h)h^2|_{h=0} = 2\int_0^\infty \gamma_t(r)\, dr \qquad (6)$$

it is possible to estimate the absolute value at zero angle of the thickness factor. From this value, in analogy to the molecular weight (eq 3), the mass per unit area can be calculated (Kratky, 1963). Thus, a value of 2500 ± 500 daltons/nm² is obtained which, assuming a bimolecular cross-section structure and a molecular weight of 678 for DMPC, results in an average area of 0.54 ± 0.09 nm²/DMPC molecule. It must be stressed, however, that this calculation involves the same sources of error as discussed above for the molecular weight. For comparison, an estimate based upon a bilayer thickness of 4.4 nm and the partial specific volume of 0.969 cm³/g yields an area of 0.49 nm²/molecule.

Table I: Structure Parameters of Dimyristoylphosphatidylcholine Vesicles Measured at 28 °C

$\bar{v}^a$	0.969 ± 0.002 cm³·g⁻¹
M^b	(3.2 ± 0.5) × 10⁶
M/nm² [c]	2500 ± 500
r^d	12 nm
d^e	4.4 nm

[a] Isopotential partial specific volume determined by precision densimetry. [b] Molecular weight determined from the absolute scattering intensity at zero angle. [c] Mass per unit area determined from the absolute value of Ih^2 at $h = 0$. [d] Average outer radius of the vesicles estimated from the distance distribution function $p(r)$. [e] Bilayer thickness obtained from the distance distribution functions $p(r)$ and $\gamma_t(r)$.

Ideally, the deconvolution of $\gamma_t(r)$ should allow a direct evaluation of the electron density distribution across the bilayer (Lesslauer et al., 1971; Weick et al., 1974; Laggner et al., 1977). Analytical procedures by which this could be performed would, however, require absolute accuracy of the function $\gamma_t(r)$. Since this is not the case and since suitable approximation procedures have not yet been developed, we prefer to evaluate the cross-section electron density profile by Fourier transformation of the thickness amplitudes $hI^{1/2}(h)$ (Figure 3b), assuming a symmetrical profile, according to the relation

$$\Delta\rho(r) = (\text{constant})\int_0^\infty hI^{1/2}(h)\cos(hr)\, dh \qquad (7)$$

Test calculations have shown that the results agree with the function $\gamma_t(r)$, which supports the assumption of a symmetrical bilayer profile within the given limits of error. Since the termination error bears more heavily on the integration in eq 7, the resulting function $\Delta\rho(r)$ is less reliable with respect to the overall bilayer thickness than the function $\gamma_t(r)$. However, the peak-to-peak distance of approximately 3.5 nm, which in reciprocal space is reflected by the position of the maxima in $I_t(h)$ and which is probably related to the cross-bilayer distance of the phosphate groups, is reliably reproduced in the function $\Delta\rho(r)$. The results in Figure 3d are given in electron density differences from the solvent ($\rho_0 = 334.5$ e/nm³) based upon the net electron density difference of 7.6 e/nm³ for DMPC vesicles.

The structure parameters of DMPC vesicles obtained from this study are summarized in Table I. It should be borne in mind that some of these values are considerably temperature dependent, especially those related to the molecular packing within the bilayer plane (Laggner, 1977). A detailed description of the thermal behavior of DMPC vesicles based upon X-ray small-angle scattering results will be given elsewhere (Laggner and Stabinger, in preparation).

Structure of the apoC-III–DMPC Complex. The uncorrected scattering curve $\tilde{I}(h)$ of a 23 mg/mL solution of an apoC-III–DMPC complex [protein/lipid, 0.26 (g/g)] is shown in Figure 4a. The relative mean error in the angular region of $h < 2$ nm⁻¹ is less than ±2%, and the maximum error in the low intensity region at higher angles is ±6%. The lower error in these data as compared to those obtained from DMPC vesicles is due to the fact that a total of 1.6×10^5 counts were

[3] The bilayer thickness d defined by the correlation function $\gamma_t(r)$ corresponds to the *maximum* dimension across the bilayer for which the electron density differs from the solvent; hence this dimension includes the water of hydration interspersed in the polar-headgroup region. This parameter is of greater physical relevance than the theoretical thickness obtained by others from the lamellar repeat distance of multilamellar dispersions through multiplication by the volume fraction of lipid. This difference in definition and the observation that the temperature dependence of the structural parameters of single-shelled vesicles is significantly different from those of multilamellar dispersions (Laggner, 1977) do not permit comparison with the structure parameters of DMPC bilayers reported by Janiak et al. (1977).

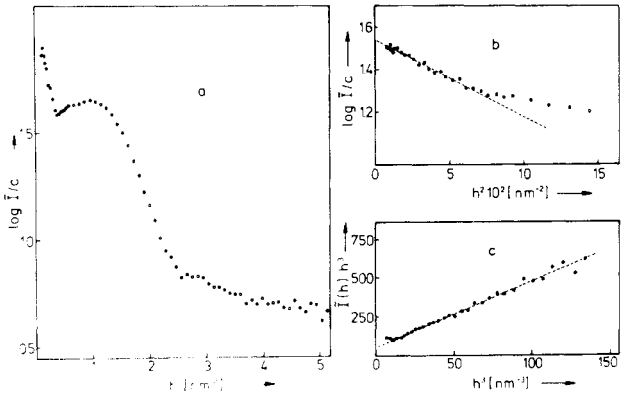

FIGURE 4: (a) Scattering intensities $\tilde{I}/c$ of a solution of apoC-III–DMPC complex (c = 23 mg/mL) with protein/lipid = 0.26 (g/g), uncorrected for the collimation geometry; T = 28 °C. Asymptotic trends of the uncorrected scattering intensities $\tilde{I}/c$ of the apoC-III–DMPC complex towards low angles (b) measured with c = 5 mg/mL and towards high angles (c) measured with c = 23 mg/mL.

accumulated at each angle in eight consecutive scans. No systematic drift of the data was observed during the time of the experiment. At the lowest angles, the scattering curve of a 5 mg/mL solution in the Guinier plot (log $\tilde{I}/c$ vs. h^2, Figure 4b) shows a linear course. In this case, unlike the results from the DMPC vesicles, the mean error from five scans during a time of 7 h is only 20% higher than the purely statistical counting error, indicating that no structural alteration took place during the experiment. The relative mean error of the intensities in Figure 4b is less than 4%. Since this measurement was performed with a relatively low sample concentration, it can be assumed that interparticle interference effects fall within the limits of error. These are, therefore, neglected. The apparent radius of gyration, $\tilde{R}$, calculated according to eq 1 is 5.0 nm. The observation of a well-defined linear Guinier range indicates that the solution is largely monodisperse. However, apart from providing evidence that the interaction of the vesicles with apoC-III has led to the formation of a new stable structural entity, the value of $\tilde{R}$ does not allow a direct structural interpretation due to the electron-density heterogeneity of the particles. Also here the outer part of the scattering curve (Figure 4c) follows an h^{-3} dependence (Porod, 1952). The constant term calculated from the slope in the $\tilde{I}h^3$ vs. h^3 plot was subtracted before desmearing of the scattering curve.

Since the maximum particle size of the complex was uncertain, the optimal choice of the value D_{max} in the desmearing procedure had to be found by trial-and-error using the approximation to the experimental data as a criterion. The greatest stability in the resulting $p(r)$ function and the best approximation were obtained for D_{max} values between 20 and 25 nm using 20, 22, and 25 Spline functions. The desmeared scattering curves found by using 20, 22.5, and 25.2 nm as D_{max} and the respective $p(r)$ functions are shown in Figure 5. The zero angle intensities $I(0)$ and the radii of gyration R calculated from the $p(r)$ functions according to

$$I(0) = 4\pi \int_0^\infty p(r)\, dr \qquad (8a)$$

and

$$R^2 = \left[\int_0^\infty p(r) r^2\, dr\right] \Big/ \left[2\int_0^\infty p(r)\, dr\right] \qquad (8b)$$

are listed in Table II.

The molecular weight of the apoC-III–DMPC complex was calculated according to eq 3 from the mean absolute value of

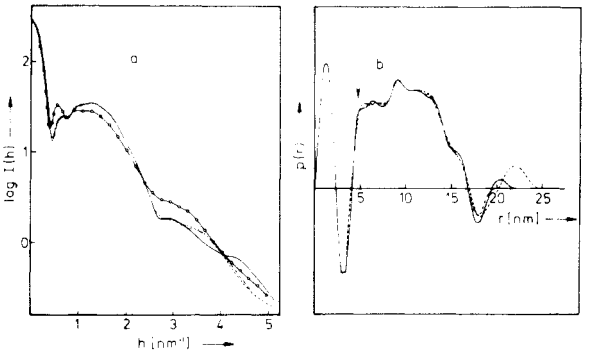

FIGURE 5: (a) Desmeared scattering curve of the apoC-III–DMPC complex calculated from the experimental data (Figure 4) assuming maximum intraparticle distances D_{max} of 20 nm (-----), 22.5 nm (—), and 25 nm (---). Dotted line: theoretical scattering curve of an oblate ellipsoidal particle with an axial ratio of 17 × 17 × 5 nm with a shell of 1-nm thickness of relative electron density ρ_{rel} = 1.0 and a core of ρ_{rel} = -0.7 (solid line). (b) Distance distribution functions $p(r)$ defined by 20, 22, and 25 cubic Spline functions in the range of 0 < r < 30 nm related to the scattering curves $I(h)$ in (a) by eq 2.

Table II: Zero Angle Scattering Intensities [$I(0)$] and Radii of Gyration (R) for the apoC-III–DMPC Complex[a]

D_{max} (nm)	$I(0)$[b]	R (nm)
20.0	279	6.65
22.5	281	6.74
25.2	293	7.21

[a] Calculated from $p(r)$, according to eq 8a and 8b. [b] Relative units.

$I(0)$ using the partial specific volume of 0.905 ± 0.003 cm^3/g measured at 28 °C. A value of M = (3.9 ± 0.4) × 10^5 was thus obtained. Since the electron density difference (Δz = 4.4 × 10^{-2} g-electrons/g) is about four times higher, the precision of M is considerably better in this case than with the DMPC vesicles. Aune et al. (1977) have reported a molecular weight of 4.42 × 10^5 for a similar preparation. Considering the methodological differences and the error involved in both approaches, these two results are in reasonable agreement. This result indicates unambiguously that the interaction with apoC-III leads to the breakdown of DMPC vesicle structure and to the formation of substantially smaller structural units. From the composition of the complex and the molecular weights of the components it follows that a single complex particle contains about nine molecules of apoC-III and 454 DMPC molecules.

It is possible to estimate the maximum particle size of the complex from the distance distribution function $p(r)$ shown in Figure 5b with better precision than in the case of the DMPC vesicles. From the crossover point near 17 nm, we estimate this dimension to be 17 ± 1 nm. The residual fluctuations at r > 17 nm are clearly due to termination effects as can be shown by model calculations simulating the present experimental angular termination at both low and high scattering angles. A comparison of this result with that for a compact sphere of 5.2 nm radius and of the same molecular weight and partial specific volume [see model I of Aune et al. (1977)] indicates that the particle must be highly asymmetric. Moreover, from the plateau in the $p(r)$ function between 5 and 13 nm (Figure 5b), it must be concluded that this asymmetry is two dimensional rather than one dimensional, i.e., the particle must be more like a platelet than a rodlike structure. In the latter case the function $p(r)$ would have to show an extended linearly decreasing course towards large values of r. The third remarkable feature of this function, the pronounced positive–negative fluctuation at r < 5 nm,

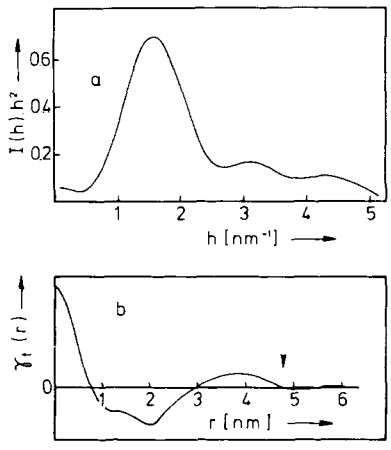

FIGURE 6: (a) Thickness factor $I(h)h^2$ of the apoC-III–DMPC complex calculated from the data in Figure 4 by assuming a one-dimensional cross-section distance distribution $\gamma_t(r)$ limited to $0 < r < D_{max}$, with $D_{max} = 6$ nm. (b) One-dimensional distance distribution function $\gamma_t(r)$ related to $I(h)h^2$ in (a) by eq 5.

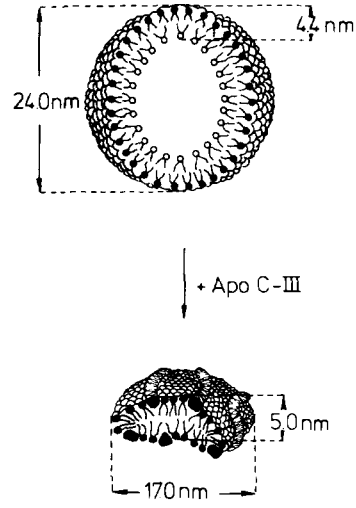

FIGURE 7: Schematic models of the DMPC vesicle (a) and the apoC-III–DMPC complex (b). At 28 °C, the DMPC vesicle has a full diameter of 24.0 nm and a bilayer width of 4.4 nm. The diameter of the internal aqueous space is 15.2 nm. The DMPC–apoC-III complex is represented as an oblate ellispoid 17.0 nm wide and 5.0 nm thick. A 1.0 nm thick shell of high electron density has been assigned to phospholipid polar head groups and apoprotein located at the periphery of the complex.

indicates that the particle must contain discrete regions of positive and negative electron density within 5 nm of each other.

From this semiquantitative discussion of the $p(r)$ function, a platelet of approximately 5-nm thickness and a maximum lateral dimension of 17 nm could be considered as consistent with the results. To refine this model, we have tried to evaluate the cross-sectional structure using the relations 4 and 5, bearing in mind, however, the rather limited degree of two-dimensional extension. The thickness factor $I(h)h^2$ and the cross-sectional correlation function $\gamma_t(r)$ were calculated directly from the experimental results employing a maximum value for D of 6 nm and using 12 Splines to define $\gamma_t(r)$ between 0 and D_{max}. To minimize influences from the overall particle size, the scattering data used for this treatment were truncated towards lower angles at $h = 10^{-2}$ nm^{-1}. The resulting thickness factor $I(h)h^2$ and the $\gamma_t(r)$ function are shown in Figure 6. A comparison of these results with those for the intact DMPC vesicle (Figure 3a,b) clearly shows characteristic similarities, and it can be inferred that the cross-sectional structure of the complex, although quantitatively different, retains significant features of the single bilayer transform. The maximum thickness of 4.9 ± 0.2 nm obtained from this result (Figure 6b) is consistent with the one inferred from the three-dimensional $p(r)$ function (arrow in Figure 5b). Without further consideration, this increase in thickness by about 0.5 nm could be ascribed to the binding of apoC-III to the external surface of the DMPC bilayer. However, apart from the fact that this would hardly explain the spontaneous breakdown of the vesicle into smaller fragments, two important considerations contradict this interpretation. First, a comparison of the volume calculated from M and $\bar{v}$ (586 nm^3) with the theoretical volume of a cylinder of 8.5-nm radius and 5-nm height (1135 nm^3) shows that such a model would be too voluminous by a factor of 2. Second, the mass per unit area calculated from the absolute value of $Ih^2(h)|_{h=0}$ (obtained from the $\gamma_t(r)$ function according to eq 6) has the value of 1400 daltons/nm^2, which represents an unreasonably low lateral packing density for a bilayer of constant thickness. These apparent inconsistencies can be overcome simply by assuming an oblate ellipsoidal structure with dimensions of 17 × 17 × 5 nm. The volume of this model is only a factor of 1.29 larger than the volume of 586 nm^3 calculated from M and $\bar{v}$. This difference, if ascribed to hydration only, would correspond to a value of 0.32 g of H_2O/g of complex. Finally, the fit between the theoretical scattering curve of an oblate ellipsoid of these overall dimensions with a 1 nm thick external shell of positive electron density and a center of negative electron density is in good agreement with the experimental scattering curve (dotted curve in Figure 5a). Alternative cylindrical models designed on the basis of radius of gyration and volume comparisons have been tested and found to be less suitable for approximating the shape of the scattering curve.

On the basis of this model, the high electron density components, i.e., phospholipid polar head groups and protein, must be situated predominantly in the outer shell of the structure, surrounding a core of fatty acyl chains. The optimum value of 1 nm for the thickness of this shell was found by trial and error. This value is in good agreement with the high electron density shell found for various high density lipoprotein species (Shipley et al., 1972; Laggner et al., 1973, 1976; Atkinson et al., 1974; Müller et al., 1974). Our results suggest there is little if any protein penetration into the hydrocarbon chain region. However, a quantitative discussion of this point is clearly beyond the limit of interpretation for our data. It is quite possible that apolar lipid–protein interaction occurs at the circumference of the ellipsoid where the low radius of curvature would otherwise lead to unfavorable exposure of hydrocarbon surfaces towards the aqueous phase (Segrest, 1977). An idealized model illustrating our molecular interpretation of the results is shown in Figure 7.

This model features the organization of the phospholipids as a micelle with the shape of an oblate ellipsoid. The apoproteins, which are 65% α-helical (Pownall et al., 1977), are embedded in the surface of this micelle. This organization would permit the hydrophobic sides of the amphipathic helical segments (Morrisett, 1977a) to face the core and interact with fatty acyl methylene groups near the carboxyl end, while the polar sides face the periphery and interact with the polar head groups. The resolution of the present X-ray scattering data makes it very difficult to distinguish between our proposed ellipsoidal model and a similar cylindrical structure which, at its periphery, is surrounded by a torus of electron dense material. However, calculations of the surface area and volume afforded by two extreme models (see Appendix) indicate that the oblate ellipsoid is favored. This model possesses

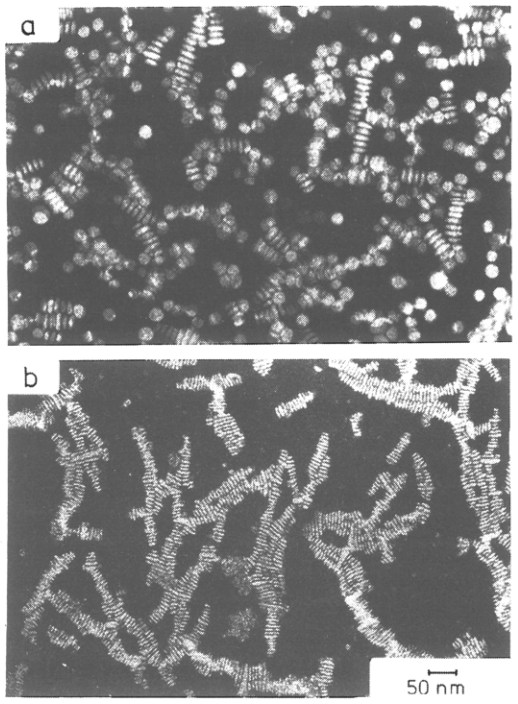

FIGURE 8: Negative stain electron micrographs of DMPC vesicles (a) and apoC-III–DMPC complexes containing 0.26 g of protein/g of lipid (b).

an area which can just accommodate the molecular components and a volume which is only 29% in excess of that required to accommodate the nine protein molecules and 545 lipid molecules in the complex. In comparison, the right cylinder exceeds the area and volume requirements of these components by 65 and 100%, respectively.

We regard the model shown in Figure 7 as a refinement of that proposed previously (Aune et al., 1977) but still not a final o e. It differs from similar ones proposed by Tall et al. (1977) and Segrest (1977) in its placement of the apoprotein, among other features. In the present model, the protein is indicated as interacting principally with the polar head regions, whereas in these other two models, the apoprotein is indicated as a belt circumscribing the exposed hydrophobic surface of the outermost hydrocarbon chains. Experiments to distinguish between these two possibilities are currently underway in our laboratories.

The present results constitute compelling evidence that the apoC-III–DMPC complex particles exist as monomers in dilute solution and do not aggregate to form what is typically observed by negative stain electron microscopy as stacked disk structures. The dimensions of the individual disks in electron micrographs are in good agreement with the present ellipsoidal model, although the size heterogeneity on the micrographs is certainly much wider (Figure 8b). The conditions of negative staining clearly favor the formation of stacklike aggregates, which is a probably unspecific phenomenon also encountered with pure DMPC vesicles (Figure 8a) and which has no significance to the situation in dilute salt solution. A qualitatively similar oblate ellipsoidal structure has been proposed for the complex formed by interaction of apoprotein from porcine high density lipoprotein and DMPC (Atkinson et al., 1976). However, in that case, the major axis is significantly shorter than in the apoC-III–DMPC complex. This structural difference may be a result of different lipid-binding capacities of the two apoproteins or different degrees of self-association which, in turn, cause a difference in distribution of the apoproteins within the complexes.

Acknowledgments

The authors are indebted to Mr. Richard Plumlee and Miss Doris Roblegg for excellent technical assistance, to Drs. Ingolic and Geymayer for obtaining the electron micrographs, to Drs. Kirk Aune, Henry Pownall, and Otto Glatter for several helpful discussions, and to Ms. Debbie Mason, Kaye Shewmaker, and Claudia Uhlich for help in preparing the manuscript.

Appendix

I. Area occupied by the individual components of the complex which contains nine apoC-III molecules and 454 DMPC molecules.

A. Area occupied by apoC-III: assumptions and calculations. (i) When bound to DMPC at 28 °C, apoC-III is 65% α-helical (Pownall et al., 1977, Figure 1a). 0.65 × 79 amino acids = 53 α-helical amino acids. The remaining 26 amino acids have chiefly random coil structure. (ii) The length of the α-helical segment is given by 53 residues × 0.15 nm/residue = 7.9 nm. (iii) The hydrophobic half of the amphipathic helix is embedded in the complex. The width of this helix (determined from space-filling models) is about 1.5 nm so the area occupied by the helical segments in the complex is given by (7.9 nm × 1.5 nm × 9 molecules)/complex = 107 nm^2. (iv) Taking a fully extended polypeptide chain as a first approximation to the random coil segments of apoC-III, the total surface area, according to the empirical relation A_t = 0.0144 × M (Teller, 1976), is

$$A_{t,C\text{-}III} = 0.33 \times 9.300 \times 9 \times 0.0144 = 398 \text{ nm}^2$$

and through multiplication by π^{-1} (ratio of longitudinal cross-section area to envelope of a cylindrical rod) the projected surface area is $A_{extended}$ = 127 nm^2. We assume that this figure is by about one-third too high due to the implied full extension of the polypeptide chain and due to its surface roughness, and therefore estimate from space-filling models the required area to accommodate the random coil portion of apoC-III to be A_{random} = 84 nm^2. (v) Total area occupied by apoC-III in one complex

$$\begin{aligned} A_{C\text{-}III} &= A_{helix} + A_{random} \\ &= 107 + 84 \\ &= 191 \text{ nm}^2 \end{aligned}$$

B. Area occupied by DMPC. (i) Molecular area of DMPC in multilayer at 37 °C (liquid–crystalline phase) is 0.608 nm^2 and at 10 °C (gel phase) is 0.502 nm^2 (Curatolo et al., 1977). (ii) Molecular area of DMPC in single bilayer vesicle at 28 °C is 0.54 nm^2. The molecular area of DMPC within the complex is unknown. Consideration of the radius of curvature for the complex and the parent vesicle suggests that the area effectively occupied by a single molecule will be larger in the former case. However, fluidity measurements (Novosad et al., 1976) suggest that some of this extra space between DMPC polar head groups may be occupied by the apoprotein. In view of these opposing effects of radius of curvature and apoprotein binding on DMPC molecular areas which cannot be readily evaluated, we have elected to use the area obtained from measurements on the vesicles. (iii) Total area of DMPC in complex will be 454 molecules × 0.54 nm^2/molecule = 245 nm^2.

C. Total area occupied by individual components

$$\begin{aligned} A_{total} &= A_{C\text{-}III} + A_{DMPC} \\ &= 191 + 245 \\ &= 436 \text{ nm}^2 \end{aligned}$$

II. Surface area of the oblate ellipsoid model (axes 17 × 17 × 5 nm)

$$a = b = 8.5 \text{ nm}$$
$$c = 2.5 \text{ nm}$$
$$A = 0.42\pi aU$$
$$= 416 \text{ nm}^2$$

where U = 37.1 nm (circumference of an ellipse, with axes 8.5 nm and 2.5 nm).

III. Surface area of a right cylinder model (r = 8.5 nm, h = 5 nm)

$$A_{cyl} = 721 \text{ nm}^2$$

Hence, the oblate ellipsoid model has a surface area very close to that estimated for the components of the complex whereas the cylindrical model exceeds this by 65%.

References

Andrews, S. B., Hoffman, R. M., & Borison, A. (1975) *Biochem. Biophys. Res. Commun. 65*, 913.

Atkinson, D., Davis, M. A. F., & Leslie, R. B. (1974) *Proc. R. Soc. London, Ser. B 186*, 165.

Atkinson, D., Smith, H. M., Dickson, J., & Austin, J. P. (1976) *Eur. J. Biochem. 64*, 541.

Aune, K. C., Gallagher, J. G., Gotto, A. M., Jr., & Morrisett, J. D. (1977) *Biochemistry 16*, 2151.

Curatolo, W., Sakura, J. D., Small, D. M., & Shipley, G. G. (1977) *Biochemistry 16*, 2313.

Glatter, O. (1977) *J. Appl. Crystallogr. 10*, 415.

Greville, T. N. E. (1969) *Theory and Applications of Spline Functions*, Academic Press, New York.

Guinier, A., & Fournet, G. (1955) *Small Angle Scattering of X-Rays*, Wiley, New York.

Jakopitsch, E., & Horn, H. (1962) *Mikroskopie 17*, 30.

Janiak, M. J., Small, D. M., & Shipley, G. G. (1977) *Biochemistry 15*, 4575.

Janosi, A., & Degovics, G. (1976) *Rep. Inst. Röntgenfeinstrukturforschung, Forschungszentrum Graz.*

Kratky, O. (1958) *Z. Elektrochem. 62*, 66.

Kratky, O. (1963) *Prog. Biophys. 13*, 105.

Kratky, O., Porod., G., & Kahovec, L. (1951) *Z. Elektrochem. Angew. Phys. Chem. 55*, 53.

Kratky, O., Porod, G., & Skala, Z. (1960), *Acta Phys. Austriaca 13*, 76.

Kratky, O., Leopold, H., & Stabinger, H. (1973) *Methods Enzymol. 27*, 98.

Laggner, P., Abstract of the 4th International Conference on Small Angle Scattering of X-Rays and Neutrons, Gatlinburg, TN, Oct 1977.

Laggner, P., & Stabinger, H. (1976) in *Colloid and Interface Science* (Kerker, M., Ed.) Vol. 5, p 91, Academic Press, New York.

Laggner, P., Müller, K., Kratky, O., Kostner, G., & Holasek, A. (1973) *FEBS Lett. 33*, 77.

Laggner, P., Müller, K., Kratky, O., Kostner, G., & Holasek, A. (1976) *J. Colloid Interface Sci. 55*, 102.

Laggner, P., Glatter, O., Müller, K., Kratky, O., Kostner, G., & Holasek, A. (1977) *Eur. J. Biochem. 77*, 165.

Leopold, H. (1968) *Z. Angew. Phys. 25*, 81.

Leopold, H. (1969) *Elektronik 11*, 350.

Lesslauer, W., Cain, J., & Blasie, J. K. (1971) *Biochim. Biophys. Acta 241*, 547.

Luzzati, V., Witz, J., & Nicolaieff, A. (1963) *J. Mol. Biol. 3*, 367.

Morrisett, J. D., Gallagher, J. G., Aune, K. C., & Gotto, A. M. (1974) *Biochemistry 13*, 4769.

Morrisett, J. D., Jackson, R. L., & Gotto, A. M. (1977a) *Biochim. Biophys. Acta 472*, 93.

Morrisett, J. D., Pownall, H. J., & Gotto, A. M. (1977b) *Biochim. Biophys. Acta 486*, 36.

Müller, K., Laggner, P., Kratky, O., Kostner, G., Holasek, A., & Glatter, O. (1974) *FEBS Lett. 40*, 213.

Novosad, Z., Knapp, R. D., Gotto, A. M., Pownall, H. J., & Morrisett, J. D. (1976) *Biochemistry 15*, 3176.

Pilz, I., & Kratky, O. (1967) *J. Colloid Interface Sci. 24*, 211.

Pilz, I., Herbst, M., & Kratky, O. (1970) *Eur. J. Biochem. 13*, 55.

Porod, G. (1948) *Acta Phys. Austriaca 2*, 255.

Porod, G. (1952) *Kolloid Z. 125*, 51.

Pownall, H. J., Morrisett, J. D., Sparrow, J. T., & Gotto, A. M. (1974) *Biochem. Biophys. Res. Commun. 60*, 779.

Pownall, H. J., Morrisett, J. D., & Gotto, A. M. (1977) *J. Lipid Res. 18*, 14.

Segrest, J. P. (1977) *Chem. Phys. Lipids 18*, 7.

Shipley, G. G., Atkinson, D., & Scanu, A. M. (1972) *J. Supramol. Struct. 1*, 98.

Tall, A. R., Small, D. M., Deckelbaum, R. J., & Shipley, G. G. (1977) *J. Biol. Chem. 252*, 4701.

Teller, D. C. (1976) *Nature (London) 260*, 729.

Träuble, H., Middelhoff, G., & Brown, V. W. (1974) *FEBS Lett. 49*, 269.

Weick, D. (1974) *Biophys. J. 14*, 233.

Wilkins, M. H. F., Blaurock, A. E., & Engelmann, D. (1971), *Nature (London), New Biol. 230*, 72.

Zipper, P. (1969) *Acta Phys. Austriaca 30*, 143.